Video Article

Optical Frequency Domain Imaging of *Ex vivo* Pulmonary Resection Specimens: Obtaining One to One Image to Histopathology Correlation

Lida P. Hariri[1,2,3], Matthew B. Applegate[4], Mari Mino-Kenudson[1,2], Eugene J. Mark[1,2], Brett E. Bouma[2,3], Guillermo J. Tearney[1,2,3], Melissa J. Suter[2,3,5]

[1]Department of Pathology, Harvard Medical School

[2]Massachusetts General Hospital

[3]Wellman Center for Photomedicine, Harvard Medical School

[4]Pulmonary and Critical Care Unit, Massachusetts General Hospital

[5]Pulmonary and Critical Care Unit, Harvard Medical School

Correspondence to: Melissa J. Suter at msuter@partners.org

URL: https://www.jove.com/video/3855
DOI: doi:10.3791/3855

Keywords: Bioengineering, Issue 71, Medicine, Biomedical Engineering, Anatomy, Physiology, Cancer Biology, Pathology, Surgery, Bronchoscopic imaging, *In vivo* optical microscopy, Optical imaging, Optical coherence tomography, Optical frequency domain imaging, Histology correlation, animal model, histopathology, airway, lung, biopsy, imaging

Date Published: 1/22/2013

Citation: Hariri, L.P., Applegate, M.B., Mino-Kenudson, M., Mark, E.J., Bouma, B.E., Tearney, G.J., Suter, M.J. Optical Frequency Domain Imaging of *Ex vivo* Pulmonary Resection Specimens: Obtaining One to One Image to Histopathology Correlation. *J. Vis. Exp.* (71), e3855, doi:10.3791/3855 (2013).

Abstract

Lung cancer is the leading cause of cancer-related deaths[1]. Squamous cell and small cell cancers typically arise in association with the conducting airways, whereas adenocarcinomas are typically more peripheral in location. Lung malignancy detection early in the disease process may be difficult due to several limitations: radiological resolution, bronchoscopic limitations in evaluating tissue underlying the airway mucosa and identifying early pathologic changes, and small sample size and/or incomplete sampling in histology biopsies. High resolution imaging modalities, such as optical frequency domain imaging (OFDI), provide non-destructive, large area 3-dimensional views of tissue microstructure to depths approaching 2 mm in real time (**Figure 1**)[2-6]. OFDI has been utilized in a variety of applications, including evaluation of coronary artery atherosclerosis[6,7] and esophageal intestinal metaplasia and dysplasia[6,8-10].

Bronchoscopic OCT/OFDI has been demonstrated as a safe *in vivo* imaging tool for evaluating the pulmonary airways[11-23] (**Animation**). OCT has been assessed in pulmonary airways[16,23] and parenchyma[17,22] of animal models and *in vivo* human airway[14,15]. OCT imaging of normal airway has demonstrated visualization of airway layering and alveolar attachments, and evaluation of dysplastic lesions has been found useful in distinguishing grades of dysplasia in the bronchial mucosa[11,12,20,21]. OFDI imaging of bronchial mucosa has been demonstrated in a short bronchial segment (0.8 cm)[18]. Additionally, volumetric OFDI spanning multiple airway generations in swine and human pulmonary airways *in vivo* has been described[19]. Endobronchial OCT/OFDI is typically performed using thin, flexible catheters, which are compatible with standard bronchoscopic access ports. Additionally, OCT and OFDI needle-based probes have recently been developed, which may be used to image regions of the lung beyond the airway wall or pleural surface[17].

While OCT/OFDI has been utilized and demonstrated as feasible for *in vivo* pulmonary imaging, no studies with precisely matched one-to-one OFDI:histology have been performed. Therefore, specific imaging criteria for various pulmonary pathologies have yet to be developed. Histopathological counterparts obtained *in vivo* consist of only small biopsy fragments, which are difficult to correlate with large OFDI datasets. Additionally, they do not provide the comprehensive histology needed for registration with large volume OFDI. As a result, specific imaging features of pulmonary pathology cannot be developed in the *in vivo* setting. Precisely matched, one-to-one OFDI and histology correlation is vital to accurately evaluate features seen in OFDI against histology as a gold standard in order to derive specific image interpretation criteria for pulmonary neoplasms and other pulmonary pathologies. Once specific imaging criteria have been developed and validated *ex vivo* with matched one-to-one histology, the criteria may then be applied to *in vivo* imaging studies. Here, we present a method for precise, one to one correlation between high resolution optical imaging and histology in *ex vivo* lung resection specimens. Throughout this manuscript, we describe the techniques used to match OFDI images to histology. However, this method is not specific to OFDI and can be used to obtain histology-registered images for any optical imaging technique. We performed airway centered OFDI with a specialized custom built bronchoscopic 2.4 French (0.8 mm diameter) catheter. Tissue samples were marked with tissue dye, visible in both OFDI and histology. Careful orientation procedures were used to precisely correlate imaging and histological sampling locations. The techniques outlined in this manuscript were used to conduct the first demonstration of volumetric OFDI with precise correlation to tissue-based diagnosis for evaluating pulmonary pathology[24]. This straightforward, effective technique may be extended to other tissue types to provide precise imaging to histology correlation needed to determine fine imaging features of both normal and diseased tissues.

Video Link

The video component of this article can be found at https://www.jove.com/video/3855/

Copyright © 2013 Journal of Visualized Experiments

Protocol

1. Imaging System

The technical details of OFDI have been described previously[4-6]. Circumferential OFDI was conducted at imaging speeds between 25 and 100 frames per second and between 512 and 2,048 axial depth profiles per circular cross-sectional image. Custom 2.4 Fr (0.8 mm diameter) helical scanning catheters used in this study were designed to operate through the access port of standard bronchoscopes. The catheters consisted of an inner optical core to focus the light onto the bronchial wall and a single-use outer sheath. The catheter body remained stationary during imaging while the inner core was rotated at a rate between 25 and 100 Hz and translated at a pullback speed of between 1.25 and 5 mm/sec. The axial resolution of the system was 6 mm in tissue and provided an image ranging depth of 7.3 mm[4-6]. Catheter-based OFDI was performed in this study to replicate *in vivo* bronchoscopic OFDI (**Figure 1**). However, this protocol may also be applied to imaging with a bench-top optical system (**Figure 3 and 4**).

2. Imaging System Set-up

1. Turn on imaging system
2. Set and record imaging parameters (rotational speed, pullback speed, image acquisition rate, etc). For the OFDI imaging system used in this study, images were obtained at 10-50 fps.
3. Attach catheter to rotary junction and pullback device.
4. Spin catheter and check for image quality. Adjust system alignment and offset as needed.

3. Tissue Preparation

1. Place a tabletop disposable absorbent pad on the benchtop and set lung specimen on pad.
2. If imaging a surgical *ex vivo* specimen from a patient, be sure to consult the pathology department to ensure that all resection margins (bronchial, vascular, and parenchymal margins) have been assessed, documented, and/or removed by a pathologist.
3. Identify the bronchial airway entering the resection specimen at the hilum. Remove any visible mucus within the airway using a syringe bore. If necessary, attach a longer segment of plastic tubing to the syringe bore to suction deeper within the airway.
4. Palpate the exterior surface of the specimen to identify the lesion of interest.
5. Using a fine metal probe, gingerly navigate through the bronchial tree until near the lesion of interest.
6. Open the airway along the probe until the lesion of interest is visible or palpable under the airway mucosa.
7. Carefully remove any blood or mucus from the airway mucosa overlying the lesion with a cotton-tipped applicator.
8. Place the OFDI catheter above the airway mucosa and obtain an image to confirm the lesion is underlying the airway mucosa and to identify a high-quality imaging region of interest for histology correlation.

4. Tissue Marking

1. Select the region of interest in the airway based on previous imaging findings in Step 3.8.
2. Choose two points on the tissue along the desired line of imaging. Points may be parallel to either the longitudinal (**Figure 2**) or circumferential (**Figure 3**) aspect of the airway, depending on desired results. Space dots no more than 1.5 cm apart so that the portion of tissue may fit in one histology block for processing. If a tissue length of > 1.5 cm is required, then split the tissue length into multiple 1.5 cm long inked regions of interest to create multiple matched imaging:histology pairs.
3. Dip a fine tipped open bore needle (*i.e.* 25 gauge 7/8" long) into the tissue marking dye (Triangle Biomedical Sciences, Durham, NC).
4. Carefully wipe excess ink off the outside of the needle with gauze, leaving tissue marking ink only within the needle bore.
5. Puncture the tissue perpendicular to the airway mucosa at the chosen point along the line of imaging.
6. Repeat steps 3.3 to 3.5 for the second point on the airway mucosa.
7. If the ink runs over the mucosal surface away from the puncture site, use a cotton tipped applicator to carefully remove the excess ink.
8. Remove mucus or blood on the surface of the airway mucosa with a cotton tipped applicator, if present.
9. If the ink dots are placed circumferentially within an airway, it is useful to pin open the two sides of the airway to flatten the tissue in the imaging field (**Figure 3a**).

5. Imaging Tissue

1. Place the OFDI catheter over each ink mark and image to ensure the marks are visible on OFDI. Marks should appear as focal disruptions within the tissue structure with overlying highly scattering particles and underlying rapid signal attenuation, which corresponds to the ink particles within the puncture site (**Figure 3b, Figure 4a, Figure 4g**).
2. If ink mark(s) are not visible on OFDI, repeat steps 4.3 to 4.7 for the non-visible marks. If ink marks are visible with OFDI, proceed to step 5.3.
3. Place the catheter parallel to the two ink marks on the airway mucosal surface such that the catheter optics overlie the tissue beyond the first ink mark (**Figure 2b**). Anchoring the proximal end of the catheter with a lightweight object and securing the distal end can help reduce motion artifacts.
4. Proceed with collecting an OFDI pullback.
5. View the OFDI pullback images to ensure both ink marks are visible in imaging and to check for motion artifacts (**Figure 3 and Figure 4**). If the marks are not visible, repeat steps 5.1 to 5.4.

Copyright © 2013 Journal of Visualized Experiments

6. Collecting and Processing Tissue

1. Place a green ink dot (Triangle Biomedical Sciences, Durham, NC) on the airway mucosal tissue to orient the beginning of the imaging scan, 0.3 cm away from the ink mark that appeared first in the imaging pullback (**Figure 2c**).
2. Remove tissue encompassing the two black ink marks and green ink mark. Trim tissue to fit into a standard histology processing cassette. If cutting fresh tissue is difficult, then the tissue may be fixed prior to removing the tissue for histology.
3. Place tissue in a histology processing cassette and fix in 10% formalin for at least 48 hr.
4. Process tissue in a tissue processor, available through any histology department.
5. Embed tissue in paraffin such that the cut sections will be parallel to the two black ink marks on the airway surface.
6. Use a tissue microtome to face the paraffin block until either an ink mark is visible or the entire tissue section is visible, whichever comes first.
7. Once both black ink marks are visible, cut one 5 µm thick section and mount onto a glass slide.
8. Continue to cut and mount 5 µm thick sections every 50 µm until the black ink marks are no longer visible or the tissue ends, whichever comes first.
9. Follow standard hematoxylin and eosin (H&E) staining protocols to stain and coverslip slides.

7. Image Processing

If images were acquired with a benchtop scanner, or other scanning technique where both ink marks were visible in a single cross-sectional image, then the image can be directly correlated with corresponding histology. If volumetric datasets were acquired with a helical scanning catheter, the images will need to be re-interpolated so that a single 2D image bisects both ink marks for correlation with histology. This can be accomplished using ImageJ or other image processing software. In some instances, the ink may not be readily visible in which case adjacent sections/slides should be examined.

Representative Results

The black ink marks should be between 1 - 1.5 cm apart to indicate the imaging region of interest. The green ink mark should be placed at the beginning of the imaging scan, before the first black ink mark to orient the specimen (**Figure 2 and Figure 3a**). Tissue ink marks should be visible on both OFDI imaging and histology (**Figure 3 and 4**). In normal swine (**Figure 3**) and human airway (**Figure 4**), typical airway layering should be visible. The epithelium (E) is visible as a thin, moderately signal dense, homogeneous layer at the luminal aspect of the airway. The lamina propria consists of organized signal-intense to signal-poor tissue, corresponding to various components of the lamina propria (LP) such as signal intense connective tissues including elastin and collagen (EL), and signal poor salivary-type glandular tissue (G). There are occasionally visible signal poor ducts (D) traversing the respiratory epithelium to connect with the bronchial lumen. Smooth muscle appears as discontinuous, interspersed smooth muscle fascicles and is thus not identifiable in OFDI. On the H&E and trichrome stains, airway layering can be visualized (**Figure 3c, 3d, 3f, 3g, 4b, 4c, 4e, and 4f**), where on trichrome the superficial dense elastic and collagenous tissues appear deep blue and the underlying smooth muscle stains red (SM). Cartilage rings (C) appear as signal poor crescent-shaped structures with well-defined boundaries, which overlap in the swine airway and do not overlap in the human airway. The perichondrium surrounding the cartilage rings appears as a thin layer of signal intense tissue encompassing the signal poor cartilage rings. In the peripheral human airways (**Figure 4g and 4h**), alveolar attachments (A) are visible as thin, signal intense lattice-like alveolar walls with signal void alveolar spaces. Vascular spaces within the lamina propria are visible as signal void linear or circular structures with mild underlying shadowing artifact (arrows).

Copyright © 2013 Journal of Visualized Experiments

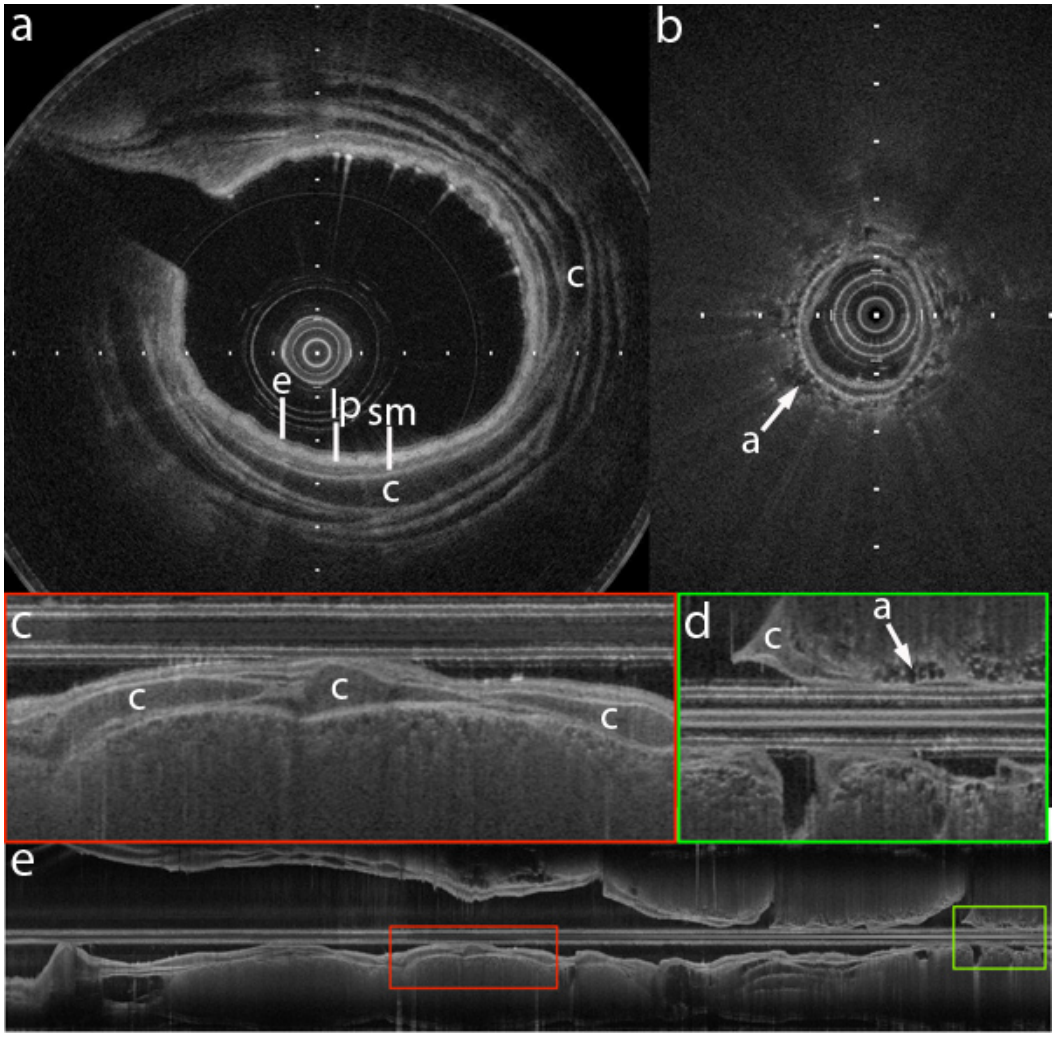

Figure 1. OFDI of swine airway. *In vivo* images obtained from a swine airway under mechanical ventilation. (a) ODFI cross-section of proximal airway. (b) OFDI cross-section of distal airway. (c) ODFI longitudinal section of proximal airway, higher magnification image of panel e in red highlighted region. (d) OFDI longitudinal section of distal airway, higher magnification image of panel e in green highlighted region. (e) ODFI longitudinal section of airway from proximal to distal (left to right). Catheter diameter is 0.8 mm and tick marks represent 0.5 mm increments. Although different layers of the airway wall and alveolar attachments are discernible in the OFDI images, it is difficult to precisely interpret the anatomic correlate of the OFDI signals without directly registered histology. e: epithelium, lp: lamina propria, sm: submucosa**,** c: cartilage, a: alveolar attachments.

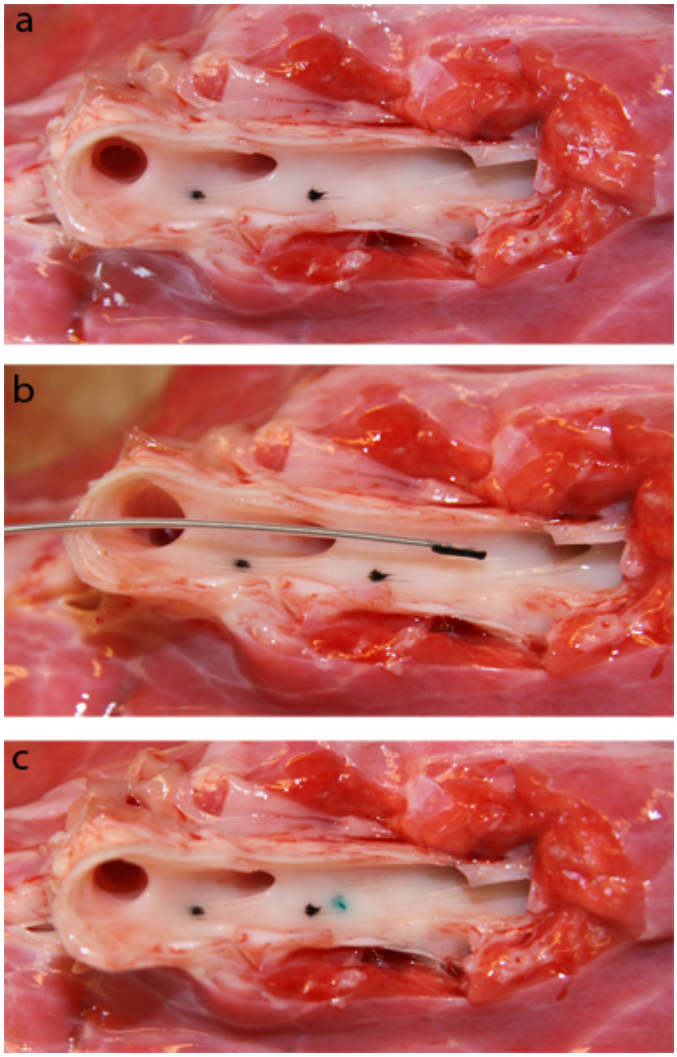

Figure 2. Tissue marking of swine airway. (a) Opened airway with two black ink marks on the luminal surface placed parallel to the longitudinal aspect of the airway, 1.5 cm apart. (b) OFDI catheter placed over two black ink marks to include both marks within the OFDI pullback. (c) Airway with additional green ink mark to orient the beginning of the imaging scan on the specimen.

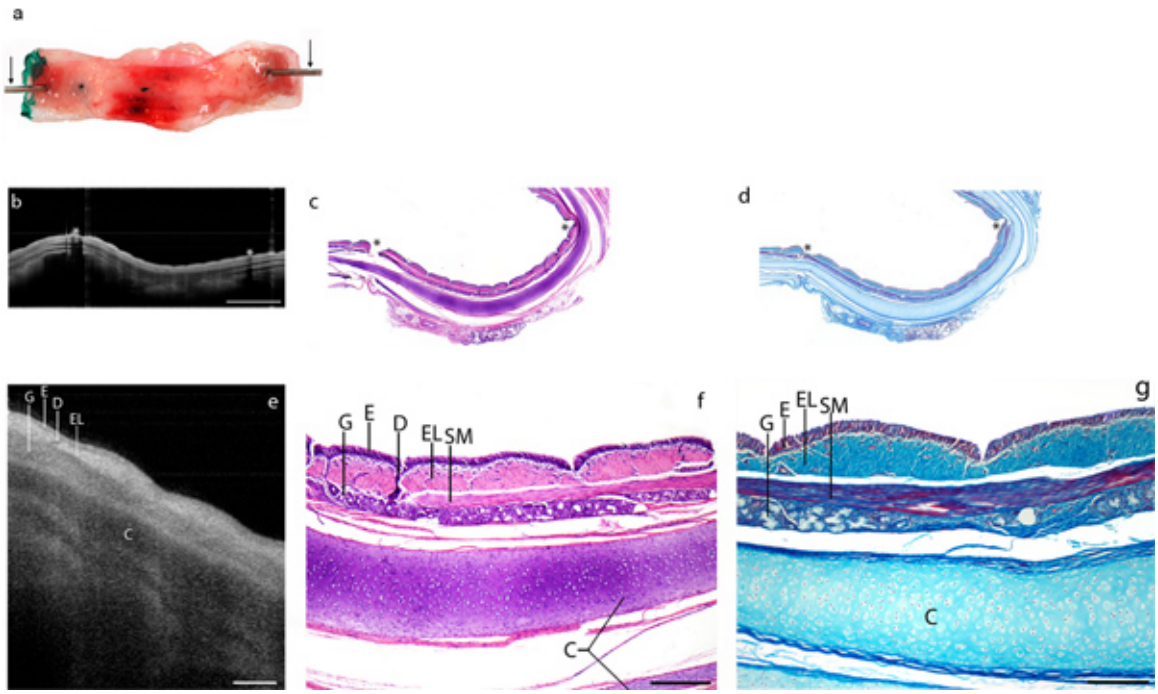

Figure 3. OFDI and histology of swine airway demonstrating precise correlation using tissue marking. (a) Opened airway with two black ink marks on the luminal surface placed parallel to the circumferential aspect of the airway. Pins are used to further open the airway (arrows). (b) OFDI of swine airway with both ink marks visible (asterisks) with (c) precisely correlated histology stained with H&E (asterisks: black ink marks visible on respiratory epithelium) and (d) correlated trichrome stain. Scale bar: 2 mm. (e) Higher magnification view of OFDI image with (f) corresponding histology stained with H&E and (g) correlated trichrome stain. E: respiratory epithelium, EL: dense collagen and elastic tissues, SM: smooth muscle, C: cartilage rings (histological artifact has resulted in artificial separation of the cartilage rings), G: salivary gland tissue, D: salivary duct entering epithelium. Scale bar: 250 μm. Click here to view larger figure.

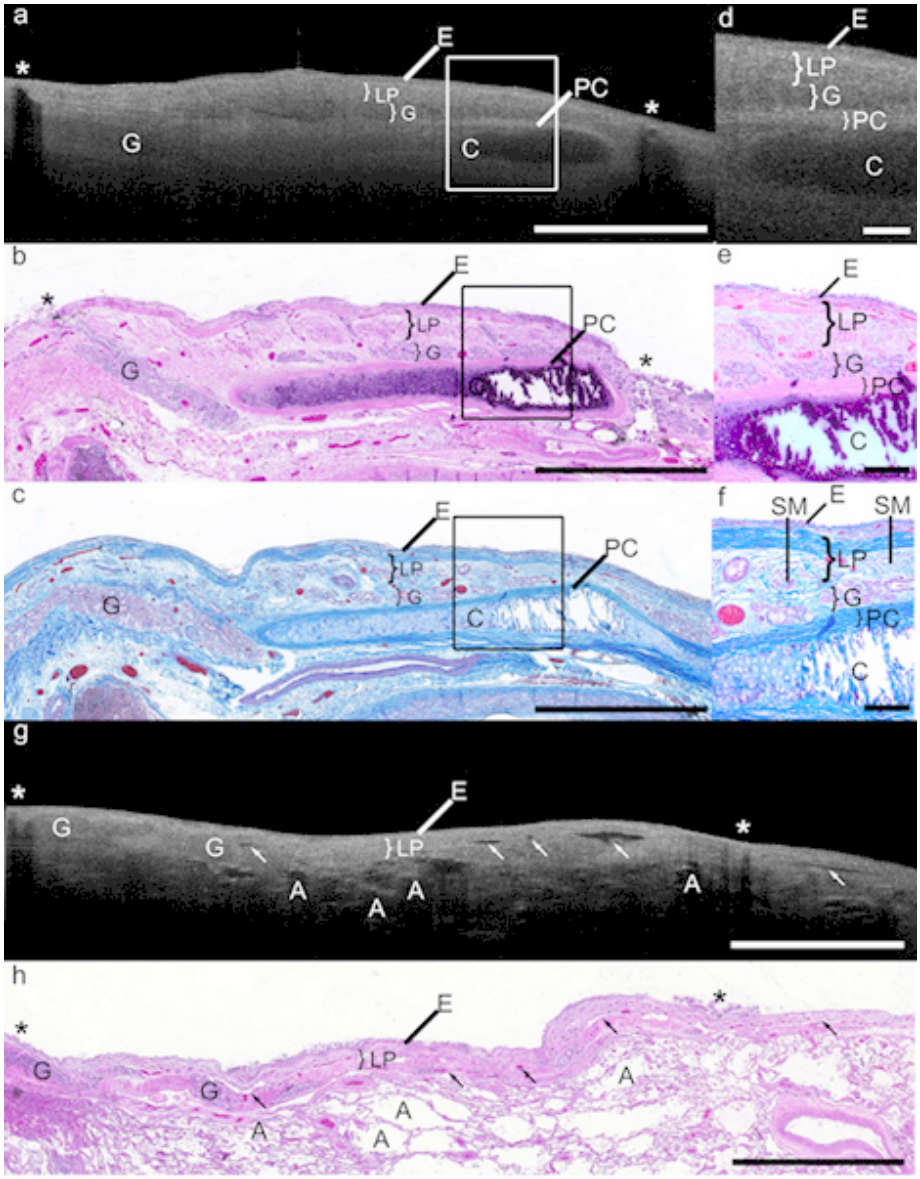

Figure 4. OFDI and histology of human airway demonstrating precise correlation using tissue marking. (a) OFDI of human proximal airway with both ink marks visible (asterisks). (b) Precisely correlated histology stained with H&E with black ink marks visible on respiratory epithelium (asterisks) and (c) correlated trichrome stain. Scale bar: 2 mm. (d) Higher magnification view of OFDI image and (e) corresponding histology stained with H&E and (f) trichrome. Scale bar: 250 μm. E: respiratory epithelium, LP: lamina propria, G: salivary gland tissue, C: cartilage rings, PC: perichondrium. In the human airway, typical layering is visible. Within the loose connective tissue, there are interspersed fascicles of red-staining smooth muscle (SM, panels c and f), which do not form a continuous band and thus are not visible as a distinct layer in OFDI. (g) OFDI of human distal airway and (h) precisely correlated H&E histology with black ink marks visible on respiratory epithelium (asterisks). Scale bar: 2 mm. Alveolar attachments (A) are visible as signal intense lattice-like alveolar walls with signal void alveolar spaces. Vascular spaces within the lamina propria are also visible as signal-void structures with underlying mild shadowing (arrows).

Discussion

Assessment of early lung malignancies can be extremely challenging due to lack of symptoms and the inability to visualize early neoplastic changes radiologically or bronchoscopically. OFDI provides near histologic resolution, large area 3-dimensional views of tissue microstructure in real time[2-6]. Endobronchial OFDI has been demonstrated in patients as a safe technique that can be used to obtain high-resolution volumetric datasets over long airway segments in the pulmonary airways[11-13] (**Animation**). However, only small biopsies are obtained as histopathological counterparts in the *in vivo* setting, which do not provide adequate correlates to OFDI for the development of imaging criteria for pulmonary pathology. In order to accurately assess OFDI features seen in pulmonary imaging, it is essential to obtain precisely matched image to histology correlations. We present a simple and effective method for precise, one to one correlation between OFDI and histology applied to airway imaging of *ex vivo* pulmonary resection specimens, which is applicable to nearly any *ex vivo* tissue type. Once imaging criteria have been established *ex vivo* with matched one-to-one histology, these criteria can then be applied to *in vivo* imaging.

Copyright © 2013 Journal of Visualized Experiments

The tissue dye used to mark the imaging region of interest is clearly visible in both OFDI and histology. By using straightforward techniques to orient the tissue, ink marks may be correlated in both imaging and histology to allow one to one comparisons of OFDI features and histology findings to determine the identifiable imaging characteristics of the tissue pathology. The technique is inexpensive and practical, thus making it useful in many optical imaging applications.

In the *in vivo* setting, methods such as laser marking may be used for tissue orientation[25]. However, the small size of the bronchial biopsy is still a limiting factor in using *in vivo* studies to develop specific imaging criteria for pulmonary pathology. Although *ex vivo* studies serve as an adequate alternate to *in vivo* imaging, there are some limitations. *Ex vivo* lung specimens are uninflated and often display surgically-induced atelectasis, which alters the appearance of normal alveolar structures. Inflating surgically resected lung tissue with tissue marking for histology correlation is technically challenging as most surgical lung specimens are received after pathology frozen section evaluation during which the pleural surface is disrupted, interfering with specimen inflation. Non-pathologic atelectasis is not an artifact seen in the *in vivo* setting, thus this limitation would not be pertinent to *in vivo* pulmonary imaging. Additionally, lack of blood within vessels in *ex vivo* specimens could make it difficult to distinguish vascular structures from other signal void structures. In the *in vivo* setting, the addition of Doppler OCT/OFDI[26-28] to structural OCT/OFDI would aid in the identification of vessels.

Motion artifacts may be seen *in vivo* where they are not present *ex vivo*. This could be potentially problematic in standard OCT systems with slower acquisition rates. However, the rapid frame rates of OFDI systems are currently > 200 fps[29-31]. Thus, it is not expected that motion artifact will be a significant issue. Previous *in vivo* OCT and OFDI imaging studies have demonstrated successful visualization of fine imaging features[14,15,18,19].

In this study we have demonstrated volumetric OFDI with precise correlation to tissue-based diagnosis for evaluating pulmonary pathology. The procedure described is intended to provide precisely matched histology to be used as gold standard for the OFDI image interpretation.

Once specific imaging criteria for pulmonary pathology have been developed and validated *ex vivo* with matched one-to-one histology, the criteria may then be applied to subsequent *in vivo* imaging studies with the use of a bronchial biopsy as a gold standard assessment of the imaging features seen. This technique is presented as an application to pulmonary resection specimens, but can be applied to almost any tissue type to provide the precise imaging to histology correlation needed to determine fine imaging features of both normal and pathological tissues.

Disclosures

Production and Free Access to this article is sponsored by NinePoint Medical Inc.

Acknowledgements

The authors would like to thank Mr. Sven Holder and Mr. Stephen Conley for their invaluable assistance in this study. This work was funded in part by the National Institute of Heath [Grant number R00CA134920] and the American Lung Association [Grant number RG-194681-N]. NinePoint Medical Inc. sponsored the publication costs associated with this manuscript.

References

1. Jemal, A., *et al.* Cancer statistics. *CA Cancer J. Clin.* **57**, 43-66 (2007).
2. Fujimoto, J.G., *et al.* Optical biopsy and imaging using optical coherence tomography. *Nat. Med.* **1**, 970-2 (1995).
3. Tearney, G.J., *et al. In vivo* endoscopic optical biopsy with optical coherence tomography. *Science.* **276**, 2037-9 (1997).
4. Yun, S., Tearney, G., de Boer, J., Iftimia, N., & Bouma, B. High-speed optical frequency-domain imaging. *Opt. Express.* **11**, 2953-63 (2003).
5. Yun, S., Tearney, G., de Boer, J., & Bouma, B. Removing the depth-degeneracy in optical frequency domain imaging with frequency shifting. *Opt. Express.* **12**, 4822-8 (2004).
6. Yun, S.H., *et al.* Comprehensive volumetric optical microscopy *in vivo. Nat. Med.* **12**, 1429-33 (2006).
7. Tearney, G.J., *et al.* Three-dimensional coronary artery microscopy by intracoronary optical frequency domain imaging. *JACC Cardiovasc. Imaging.* **1**, 752-61 (2008).
8. Suter, M.J., *et al.* Image-guided biopsy in the esophagus through comprehensive optical frequency domain imaging and laser marking: a study in living swine. *Gastrointest. Endosc.* **71**, 346-53 (2010).
9. Suter, M.J., *et al.* Comprehensive microscopy of the esophagus in human patients with optical frequency domain imaging. *Gastrointest. Endosc.* **68**, 745-53 (2008).
10. Desjardins, A.E., *et al.* Angle-resolved optical coherence tomography with sequential angular selectivity for speckle reduction. *Optics express.* **15**, 6200-9 (2007).
11. Lam, S., *et al. In vivo* optical coherence tomography imaging of preinvasive bronchial lesions. *Clin. Cancer Res.* **14**, 2006-11 (2008).
12. Michel, R.G., Kinasewitz, G.T., Fung, K.M., & Keddissi, J.I. Optical coherence tomography as an adjunct to flexible bronchoscopy in the diagnosis of lung cancer: a pilot study. *Chest.* **138**, 984-8 (2010).
13. Williamson, J.P., *et al.* Using optical coherence tomography to improve diagnostic and therapeutic bronchoscopy. *Chest.* **136**, 272-6 (2009).
14. Coxson, H.O. & Lam, S. Quantitative assessment of the airway wall using computed tomography and optical coherence tomography. *Proc. Am. Thorac. Soc.* **6**, 439-43 (2009).
15. Coxson, H.O., *et al.* Airway wall thickness assessed using computed tomography and optical coherence tomography. *Am. J. Respir. Crit. Care Med.* **177**, 1201-6 (2008).
16. Hanna, N., *et al.* Two-dimensional and 3-dimensional optical coherence tomographic imaging of the airway, lung, and pleura. *J. Thorac. Cardiovasc. Surg.* **129**, 615-22 (2005).
17. Quirk, B.C., *et al. In situ* imaging of lung alveoli with an optical coherence tomography needle probe. *J. Biomed. Opt.* **16**, 036009 (2011).
18. Su, J., *et al.* Real-time swept source optical coherence tomography imaging of the human airway using a microelectromechanical system endoscope and digital signal processor. *J. Biomed. Opt.* **13**, 030506 (2008).

Copyright © 2013 Journal of Visualized Experiments

19. Suter, M.J., *et al.* Real-time Comprehensive Microscopy Of The Pulmonary Airways: A Pilot Clinical Study. *Am. J. Respir. Crit. Care Med.* **181**, A5159 (2010).
20. Tsuboi, M., *et al.* Optical coherence tomography in the diagnosis of bronchial lesions. *Lung Cancer.* **49**, 387-94 (2005).
21. Whiteman, S.C., *et al.* Optical coherence tomography: real-time imaging of bronchial airways microstructure and detection of inflammatory/neoplastic morphologic changes. *Clin. Cancer Res.* **12**, 813-8 (2006).
22. Xie, T., *et al. In vivo* three-dimensional imaging of normal tissue and tumors in the rabbit pleural cavity using endoscopic swept source optical coherence tomography with thoracoscopic guidance. *J. Biomed. Opt.* **14**, 064045 (2009).
23. Yang, Y., *et al.* Use of optical coherence tomography in delineating airways microstructure: comparison of OCT images to histopathological sections. *Phys. Med. Biol.* **49**, 1247-55 (2004).
24. Hariri, L.P., *et al.* Volumetric optical frequency domain imaging of pulmonary pathology with precise correlation to histopathology. *CHEST.*, In Press, (2012).
25. Suter, M.J., *et al.* Image-guided biopsy in the esophagus through comprehensive optical frequency domain imaging and laser marking: a study in living swine. *Gastrointestinal endoscopy.* **71**, 346-53 (2010).
26. Chen, Z., *et al.* Noninvasive imaging of *in vivo* blood flow velocity using optical Doppler tomography. *Optics letters.* **22**, 1119-21 (1997).
27. Osiac, E., Saftoiu, A., Gheonea, D.I., Mandrila, I., & Angelescu, R. Optical coherence tomography and Doppler optical coherence tomography in the gastrointestinal tract. *World journal of gastroenterology : WJG.* **17**, 15-20 (2011).
28. Yang, V.X., *et al.* Endoscopic Doppler optical coherence tomography in the human GI tract: initial experience. *Gastrointestinal endoscopy.* **61**, 879-90 (2005).
29. Braaf, B., *et al.* Phase-stabilized optical frequency domain imaging at 1-microm for the measurement of blood flow in the human choroid. *Opt. Express.* **19**, 20886-903 (2011).
30. Oh, W.Y., Vakoc, B.J., Shishkov, M., Tearney, G.J., & Bouma, B.E. >400 kHz repetition rate wavelength-swept laser and application to high-speed optical frequency domain imaging. *Opt. Lett.* **35**, 2919-21 (2010).
31. Gora, M., *et al.* Ultra high-speed swept source OCT imaging of the anterior segment of human eye at 200 kHz with adjustable imaging range. *Opt. Express.* **17**, 14880-94 (2009).

Copyright © 2013 Journal of Visualized Experiments